

Excited State Intramolecular Proton Transfer of New Diphenylethylene Derivatives Bearing Imino Group: A Combination of Experimental and Theoretical Investigation

Gao, Fang*(高放) Zhong, Xiaolin(仲晓林) Wang, Qi(王琪)
Li, Hongru*(李红茹) Zhang, Shengtao(张胜涛)

College of Chemistry and Chemical Engineering, Chongqing University, Chongqing 400044, China

In this paper, we described the synthesis and characterization of new diphenylethylene bearing imino group. We concentrated particularly on the investigation of the possibility of the excited state intramolecular charge transfer (ESIPT) of the new dyes experimentally and theoretically. The absorption and fluorescence spectroscopy of the dyes were determined in various solvents. The results showed that the maximal absorption wavelength of 2-[(4'-*N,N*-dimethylamino-diphenylethylene-4-ylimino)methyl]phenol (**C1**) and 4-[(4'-*N,N*-dimethylamino-diphenylethylene-4-ylimino)methyl]phenol (**C2**) exhibited almost independence on the solvent polarity. While as contrast, the maximal fluorescence wavelength of the dyes showed somewhat dependence on the solvent polarity. In particular, **C1** displayed well-separated dual fluorescence spectroscopy. The second fluorescence peak was characterized with an "abnormal" fluorescence emission wavelength in aprotic solvents with large Stokes shift (*ca.* 140 nm in THF), which was much more than normal Stokes shift (*ca.* 30 nm in THF). This emission spectroscopy could be assigned to ESIPT emission. On the other hand, the ESIPT fluorescence of **C1** was much reduced or lost in the protic solvents. While, only normal fluorescence emission was detected in various solvents. Although the absorption maxima of **C1** exhibited about 10 nm red-shift with respect to those of **C2**, the normal fluorescence maxima of **C1** and **C2** were almost identical in various solvents. These results suggested that **C1** could undergo ESIPT, but **C2** was not able to proceed ESIPT. The molecular geometry optimization of phototautomers in the ground electronic state (S_0) was carried out with HF method (Hartree-Fock) and at DFT level (Density Functional Theory) using B3LYP both, while the CIS was employed to optimize the geometries of the first singlet excited state (S_1) of the phototautomers of **C1** and **C2** respectively. The properties of the ground state and the excited state of the phototautomers of **C1** and **C2**, including the geometrical parameter, the energy, the frontier orbitals, the Mulliken charge and the dipole moment change were performed and compared completely. The data were analyzed further based on our experimental results. Furthermore, the absorption and fluorescence spectra were calculated in theory and compared with the measured ones. The rate constant of internal proton transfer ($9.831 \times 10^{11} \text{ s}^{-1}$) of **C1** was much lower than that of salicylidene methylamine (**C3**, $2.045 \times 10^{15} \text{ s}^{-1}$), which was a typical Schiff base compound and was well demonstrated to undergo ESIPT easily under photoexcitation.

Keywords excited state intramolecular charge transfer (ESIPT), dye, imino group, synthesis, theoretical calculation, density functional theory (DFT), spectroscopy

Introduction

Photoinduced excited state intramolecular proton transfer (ESIPT) reaction is believed to be greatly important photoreaction in chemical and biological systems and has received considerable attention in experiment and theory.¹⁻¹⁰ Normally, an ESIPT molecule is characterized with an exceptionally and anomalously large Stokes shift, which has been found in many varieties of applications including photochromic material,¹¹ laser dyes,¹² ultraviolet photostabilizers,¹³ fluorescence probe,¹⁴ electroluminescent materials¹⁵ and so on.¹⁶⁻¹⁸

This is achieved by an ultrafast photoinduced tautomerization process between enol form and keto form when the intramolecular H-bonded molecule is photoexcited, which is characterized with four-level cycle reaction occurring via five or six members ring.¹⁹ The stable ground state in the enol form and the stable excited state in the keto form result in the absorption from $E \rightarrow E^*$ and the emission from $K^* \rightarrow K$, causing an abnormally large Stokes shift without self-absorption.²⁰

Numerous ESIPT molecules have been discovered and developed to deeply understand the photophysics

* E-mail: fanggao1971@gmail.com

Received November 18, 2009; revised and accepted March 23, 2010.

Project supported by the National Natural Science Foundation of China (Nos. 20776165, 20702065 and 20872184), Natural Science Foundation of CQ CSTC (Nos. CSTC 2009BB4216) and the Key Foundation of Chongqing Science and Technology Commission (No. CSTC 2008BA4020).

and photochemistry.^{21–24} Most of such molecules have small chemical structures so the occurrence of ESIPT is barrierless or with negligible barrier. It is quite difficult to look for an ESIPT reaction with a finite and well-defined barrier although this is significantly important to gain detailed insights into the reaction potential energy surfaces.²⁵ It is not clear that if the internal proton transfer process in the excited state including the electron density distribution of frontier orbitals, the potential energy surface, and the reaction rate constant and so on could be mediated by the molecular size yet. Hence, it stimulates the development of new ESIPT molecules with large chemical structures. On the other hand, the molecular design and huge computations are two major challenges for organic and physical chemists. Only a few investigations on the ESIPT of large molecules were reported in experimental investigation.^{26–28} For instance, Yang *et al.*²⁶ observed the aggregation-induced ESIPT emission enhancement of some large molecules, and Park *et al.*^{27,28} demonstrated that a few dendritic polyether molecules were able to undergo ESIPT emission as photoexcitation. Experimental and theoretical investigation on the occurrence of ESIPT of large molecules becomes very necessary. One of the central subjects is whether the reaction process of ESIPT is influenced by the molecular size. The results would certainly answer if the ESIPT has relationship with the chromophore parts in the molecule accordingly, and they could provide the guidance on the design and synthesis of molecules with ESIPT for various applications.

ESIPT presenting in the Schiff bases makes them attractive compounds for theoretical and experimental investigations.^{29–31} It was well demonstrated that salicylidene methylamine could undergo ESIPT easily via barrierless process.³² Aiming at revealing the effect of molecular size on the occurrence of ESIPT of molecules, new dyes with imino group was designed and synthesized, in which salicylidene methylamine was used as ESIPT parent moiety. The spectroscopic properties of new dyes were investigated in various solvents. Furthermore, the ESIPT process was calculated by the DFT (Density Functional Theory), HF (Hartree-Fock), TDDFT (time-dependent DFT) and CIS (Configuration Interaction Singles-excitation) and compared with the experimental results.

Experimental and calculation

Reagents and materials

Organic solvents were obtained from Chongqing Medical and Chemical Corporation. Other chemicals and reagents were purchased from Aldrich unless otherwise specified. The organic solvents were dried using standard laboratory techniques according to the published methods.³³ The starting materials were further purified with redistillation or recrystallization before use. 2-[(4'-*N,N*-Dimethylamino-diphenylethylene-4-ylimino)-

methyl]phenol (**C1**) and 4-[(4'-*N,N*-dimethylamino-diphenylethylene-4-ylimino)methyl]phenol (**C2**) were synthesized in our laboratory (Figure 1).

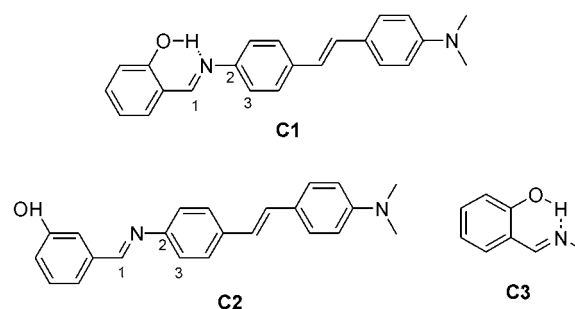


Figure 1 Chemical structure of the title compounds with some atom numbering.

Instruments

The UV/visible absorption spectra ($1 \times 10^{-5} \text{ mol} \cdot \text{L}^{-1}$) were recorded with a Cintra spectrophotometer. The emission spectra ($1 \times 10^{-5} \text{ mol} \cdot \text{L}^{-1}$) were checked with Shimadzu RF-531PC spectrofluorophotometer. Quinine sulfate in $0.5 \text{ mol} \cdot \text{L}^{-1} \text{ H}_2\text{SO}_4$ ($\Phi = 0.546$, $1 \times 10^{-6} - 1 \times 10^{-5} \text{ mol} \cdot \text{L}^{-1}$) was used as a reference to determine the fluorescence quantum yields of the compounds herein.³⁴ To avoid self-quenching of fluorescence emission, low concentration of the samples ($1 \times 10^{-6} \text{ mol} \cdot \text{L}^{-1}$) was prepared for the survey of fluorescence quantum yields. The melting point was recorded using a Beijing Fukai melting point apparatus. Nuclear magnetic resonance (NMR) spectroscopy was conducted at room temperature on a Bruker 500 MHz apparatus with tetramethylsilane (TMS) as an internal standard and CDCl_3 as solvent. Elemental analysis was performed by a CE440 elemental analysis meter from Exeter Analytical Inc.

The fluorescence quantum yields of the compounds in solvents with different polarities were measured based on the following equation [Eq. (1)]:^{35,36}

$$\Phi_f = \Phi_f^0 \frac{n_0^2 A^0 \int I_f(\lambda_f) d\lambda_f}{n^2 A \int I_f^0(\lambda_f) d\lambda_f} \quad (1)$$

wherein n_0 and n are the refractive indices of the solvents, A^0 and A are the optical densities of the reference and the sample at excitation wavelength respectively, Φ_f and Φ_f^0 are the quantum yields of the reference and the sample at excitation wavelength respectively, and the integrals denote the area of the fluorescence bands for the reference and sample, respectively.

Theoretical calculations

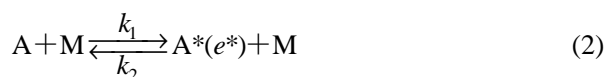
The calculations were performed by means of the Gaussian 03 program package. The physical condition was supposed in vacuum. The geometry optimization of enol and keto forms for the ground electronic state (S_0) was carried out with HF method and at the DFT level

using the B3LYP both,³⁷⁻³⁹ while the CIS has been employed to optimize the geometries of the first singlet excited state (S_1) of the two tautomers of **C1** and **C2**.

Although the CIS method has been shown to produce basically reliable geometries and force-fields, it predicts too much high excitation energies (*ca.* 1 eV).³⁷ To correct the errors and introduce the dynamic electron correlation, DFT and TDDFT were performed to predict energies at the HF and CIS optimized geometries for S_0 and S_1 state respectively, such as DFT//HF or TDDFT//CIS (denoted as single-point calculation//optimization method), the latter was used to analyze the fluorescence properties of the tautomer in the excited state. The TDDFT//HF and TDDFT//DFT were used for the calculation of absorption spectra.

The geometries of transition state (TS) were located using the synchronous transit-guided quasi Newton (QST2) method. Frequency calculations using the same methods as those for geometry optimization were performed for the obtained structure. All real frequencies have confirmed the presence of the local minimum, while one imaginary frequency indicated the existence of a transition state. All calculations were carried out with 6-31G** basis set.

To further understand the proton transfer reaction, the proton transfer rate constants in the ground and the excited state were calculated with RRKM (Rice-Ramsperger-Kassel-Marcus) theory.^{40,41} This theory amended the Lindemann process, which described the expression of a unimolecular reaction as:



where A^* is called as energized molecule and it has sur-

plus energy e^* , generally speaking, it is produced by the collision between A and M. But in the ESIPT process, the energy is obtained by proton excitation. If A^* converts into the product P, it has to overcome the energy barrier and pass the transition state form A^\ddagger .

When reaction Eq. (2) reaches the steady-state, the rate constant $k_3(e^*)$ can be written as:

$$k_3(e^*) = k^\ddagger \frac{[A^\ddagger]}{[A^*]} \quad (4)$$

which is the starting point for the calculated rate constant with RRKM theory. And the last result will be obtained by the integral of all energies.

$$k = \int_{E_0}^{\infty} \frac{k_{-1}k_2(e^*)f(e^*)[M]}{k_2(e^*) + k_{-1}[M]} de^* \quad (5)$$

Considering that the ESIPT process happens in the solution, high pressure condition is selected, $[M] \rightarrow \infty$, and Eq. (4) can be reduce to transition state theory as

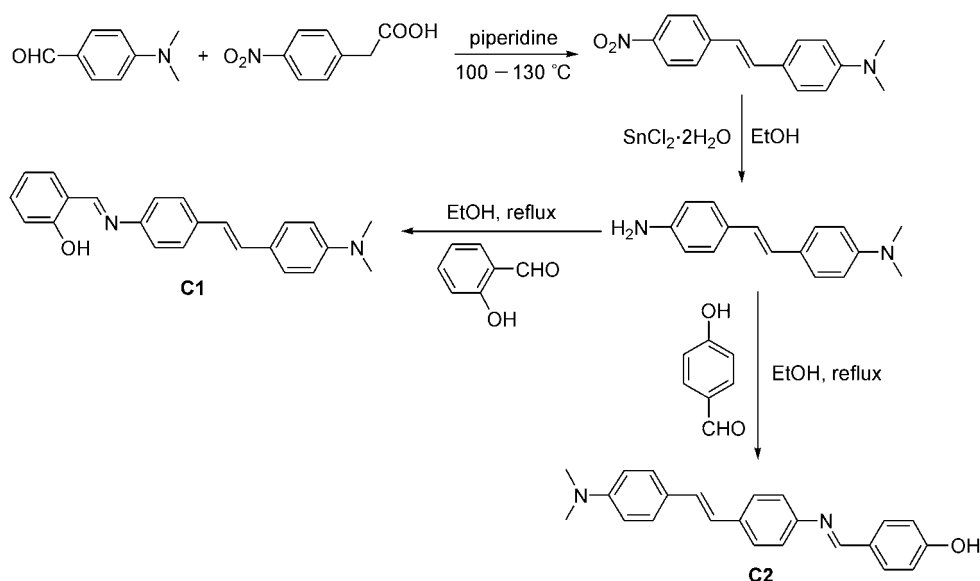
$$k = \frac{k_B T}{h} \cdot \frac{q^\ddagger}{q_A} \cdot \exp(-E_0 / RT) \quad (6)$$

Synthesis

The synthesis routes of **C1** and **C2** were shown in Scheme 1.

***p*-Nitro-*p'*-*N,N*-dimethylamino-stilbene** The title compound was synthesized according to a similar procedure with modified procedure.⁴² *p*-Nitro-phenylacetic acid (5.466 g, 30 mmol) and *p*-dimethylaminobenzaldehyde (3 g, 20 mmol) were mixed fully and piperidine (2.54 g, 3 mL) was added into the reactant. The resulting mixture was heated at 100 °C for 2 h till a black solid was formed. The product (3.24 g, yield 61%) was

Scheme 1 The synthesis routes of **C1** and **C2**



obtained as a deep red solid after twice recrystallization in alcohol. Color: deep red, m.p. 234–235 °C; ^1H NMR (CDCl_3 , 500 MHz) δ : 3.00 [s, 6H, Ar-N(CH₃)₂], 6.71 (d, $J=8.5$ Hz, 2H, ArH), 6.93 (d, $J=16.0$ Hz, 1H, Ar-CH=CH-Ar), 7.21 (d, $J=16.0$ Hz, 1H, Ar-CH=CH-Ar), 7.45 (d, $J=8.5$ Hz, 2H, ArH), 7.56 (d, $J=9.0$ Hz, 2H, ArH), 8.18 (d, $J=9.0$ Hz, 2H, ArH). Anal. calcd for C₁₆H₁₆N₂O: C 71.62, H 6.01, N 10.44; found C 71.57, H 5.96, N 10.53.

***p*-Amino-*p'*-*N,N*-dimethylamino-stilbene** *p*-Nitro-*p'*-*N,N*-dimethylamino-stilbene (1 g, 3.731 mmol) was dissolved in 100 mL anhydrous ethanol. Under argon atmosphere, stannous chloride dehydrate (1.684 g, 7.462 mmol) was added slowly. The mixture was kept refluxed for 24 h and then concentrated in vacuum. The solid was dissolved in 15% sodium hydroxide solution and its pH was adjusted to 8–9 with the dilute hydrochloric acid solution. Brown solid was obtained after filtration, and then it was washed by the distilled water for three times (30 mL \times 3), which was further purified with column chromatography using methylene chloride as eluent. Yield 46%, m.p. 160–162 °C; Color: yellowish brown; ^1H NMR (Benzene-*d*₆, 500 MHz) δ : 2.63 [s, 6H, N(CH₃)₂], 6.45 (d, $J=8.5$ Hz, 2H, ArH), 6.72 (d, $J=8.5$ Hz, 2H, ArH), 7.264 (s, 2H, Ar-CH=CH-Ar), 7.41 (d, $J=8.5$ Hz, 2H, Ar-H), 7.55 (d, $J=9.0$ Hz, 2H, ArH). Anal. calcd for C₁₆H₁₈N₂: C 80.63, H 7.61, N 11.75; found C 80.59, H 7.52, N 11.83.

2-[(4'-*N,N*-Dimethylamino-diphenylethylene-4-ylimino)methyl]phenol (C1) *p*-Nitro-*p'*-*N,N*-dimethylamino-stilbene (0.100 g, 0.42 mmol) was dissolved in 30 mL absolute ethanol. *o*-Hydroxy-benzaldehyde (0.051 g, 0.42 mol) was added into the mixture slowly under argon atmosphere. The reactant was kept refluxed for 3 h. After cooling, yellow solid was precipitated and filtered and washed with anhydrous alcohol three times (30 mL per time). 0.1 g product was obtained after twice recrystallization in ethanol. Yield 68%, m.p. 233–234 °C; Color: orange yellow; ^1H NMR (CDCl_3 , 500 MHz) δ : 3.00 [s, 6H, Ar-N(CH₃)₂], 6.75 (s, 2H, ArH), 6.91–6.99 (m, 2H, Ar-CH=CH-Ar), 7.01–7.08 (m, 2H, ArH), 7.28 (d, $J=8.5$ Hz, 2H, ArH), 7.35–7.40 (m, 2H, ArH), 7.43 (d, $J=8.5$ Hz, 2H, ArH), 7.53 (d, $J=8.5$ Hz, 2H, ArH), 8.76 (s, 1H, Ar-CH=N-Ar), 13.34 (s, 1H, Ar-OH). Anal. calcd for C₂₃H₂₂N₂O: C 80.67, H 6.48, N 8.18; found C 80.78, H 6.39, N 8.27.

4-[(4'-*N,N*-Dimethylamino-diphenylethylene-4-ylimino)methyl]phenol (C2) The synthesis is similar to that of **C1** except for *p*-hydroxy-benzaldehyde as starting material. Yield 53%, m.p. 237–238 °C; Color: dark yellow; ^1H NMR (DMSO-*d*₆, 500 MHz) δ : 2.93 [s, 6H, Ar-N(CH₃)₂], 6.72 (d, $J=7.5$ Hz, 2H, ArH), 6.88 (d, $J=8.5$ Hz, 2H, ArH), 6.98 (d, $J=17.0$ Hz, 1H, Ar-CH=CH-Ar), 7.11 (d, $J=16.0$ Hz, 1H, Ar-CH=CH-Ar), 7.21 (d, $J=7.0$ Hz, 2H, Ar-H), 7.40 (t, $J=18.0$ Hz, 2H, Ar-H), 7.54 (d, $J=8.0$ Hz, 2H, Ar-H), 7.77 (d, $J=8.0$ Hz, 2H, Ar-H), 8.51 (s, 1H, Ar-CH=N-Ar), 10.13

(s, 1H, ArOH); ^{13}C NMR (DMSO-*d*₆, 125 MHz) δ : 112.734, 116.123, 121.852, 123.653, 125.578, 127.096, 127.915, 128.130, 128.530, 131.081, 135.812, 150.381, 150.599, 159.490, 161.031. Anal. calcd for C₂₃H₂₂N₂O: C 80.67, H 6.48, N 8.18; found C 80.75, H 6.52, N 8.09.

Results and discussion

General remarks

The occurrence of ESIPT of a molecule is driven by the electron density redistribution induced by photoexcitation, which is accompanied by the large changes in the acidity or basicity of the “ESIPT groups”.⁴³ Normally, this process is completed barrierlessly or nearly barrierlessly through a five or six-members ring state. Thus, we anticipated that **C1** could be able to undergo ESIPT process with appreciable barrier via a six-member ring state, while **C2** would have to go through an eight-member ring state if it underwent ESIPT process. It meant that phenyl ring had to be twisted if eight-member ring state was formed. Consequently, it would be reasonable to expect the existence of a too large energy barrier for **C2**. Hence, the occurrence of ESIPT would be barely. While as contrast, **C1** was able to undergo ESIPT process with appreciable barrier via a reasonable six-member ring state.

Spectroscopic properties

Absorption spectroscopy A typical comparison of the absorption spectroscopy of **C1** and **C2** in ethyl acetate was presented in Figure 2. Clearly, **C1** and **C2** exhibited similar absorption spectroscopy from 275 to 500 nm. The maximal absorption of the compounds could be from overall molecular (π , π^*) transition.⁴⁴ The maximal absorption wavelength and the molar extinction coefficients of **C1** and **C2** in various solvents are listed in Table 1. The data showed that the maximal absorption wavelength of **C1** displayed approximate 10 nm bathochromic shift with respect to **C2** in various solvents. Furthermore, the maximal absorption wavelength of **C1** and **C2** exhibited very small change in different solvents. In other words, the absorption spectra of **C1** and **C2** were weakly dependent on the solvent polarity and the absorption maxima were less sensitive to the solvent polarity.

Fluorescence spectroscopy As expected, **C1** and **C2** exhibited remarkably different fluorescence spectroscopy. **C1** showed well-separated dual fluorescence emission in aprotic solvents, while **C2** displayed single fluorescence emission band in various solvents. In low-polar solvents, the fluorescence emission of **C1** and **C2** generally showed a shoulder peak. A typical comparison of the fluorescence spectroscopy of **C1** and **C2** in ethyl acetate is shown in Figure 3. The first emission band of **C1** was almost identical to the fluorescence spectroscopy of **C2**. They were effectively the same as the S₀→S₁ absorption spectral feature, which demon-

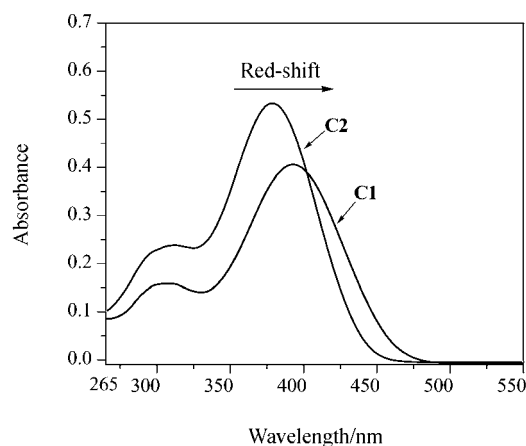


Figure 2 Ultraviolet/visible absorption spectroscopy of **C1** and **C2** in ethyl acetate ($c=1 \times 10^{-5} \text{ mol}\cdot\text{L}^{-1}$).

Table 1 The maximal absorption wavelength and molar extinction coefficients of **C1** and **C2** in various solvents^a

Solvent		C1	C2
Cyclohexane	$\lambda_{a,max}/\text{nm}$	391.2	
	ϵ	0.323	
Benzene	$\lambda_{a,max}/\text{nm}$	395.4	384.0
	ϵ	0.379	0.307
1,4-dioxane	$\lambda_{a,max}/\text{nm}$	395.3	380.8
	ϵ	0.387	0.446
Tetrahydrofuran	$\lambda_{a,max}/\text{nm}$	396.0	379.2
	ϵ	0.274	0.463
Ethyl Acetate	$\lambda_{a,max}/\text{nm}$	392.8	378.5
	ϵ	0.410	0.518
Methylene chloride	$\lambda_{a,max}/\text{nm}$	397.2	384.8
	ϵ	0.537	0.498
Acetonitrile	$\lambda_{a,max}/\text{nm}$	392.4	383.2
	ϵ	0.437	0.609
Acetone	$\lambda_{a,max}/\text{nm}$	395.8	380.8
	ϵ	0.462	0.569
Methanol	$\lambda_{a,max}/\text{nm}$	391.3	379.0
	ϵ	0.502	0.799
Ethanol	$\lambda_{a,max}/\text{nm}$	392.0	379.4
	ϵ	0.494	0.418

^a ϵ : $10^5 \text{ mol}^{-1}\cdot\text{cm}^{-1}$, $c(\mathbf{C1})=c(\mathbf{C2})=1 \times 10^{-5} \text{ mol}\cdot\text{L}^{-1}$, $\lambda_{a,max}$: the maximal absorption wavelength.

strated that both the emissions originated from similar ground state precursor. The second fluorescence emission band of **C2** was much red-shifted with respect to the first one. The first emission peak of **C1** could be the normal emission fluorescence because it exhibited a normal Stokes shift (*ca.* 30 nm in THF). While as contrast, the second fluorescence peak of **C1** showed anomalously large Stokes-shifted (*ca.* 140 nm in THF).

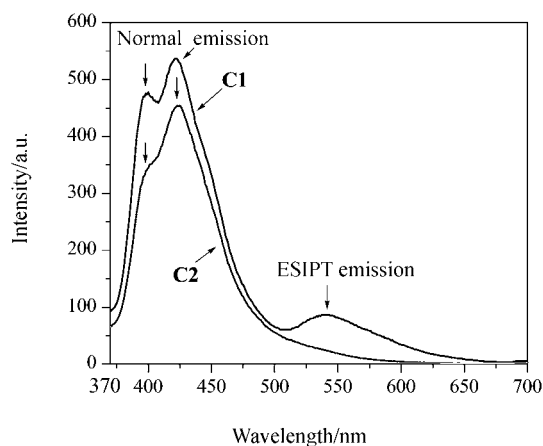


Figure 3 The fluorescence spectroscopy of **C1** and **C2** in ethyl acetate ($c=1 \times 10^{-5} \text{ mol}\cdot\text{L}^{-1}$). Ex: 350 nm, Slit window: Ex: 5 nm, Em: 5 nm.

Thus, we could conclude that ESIPT took place in **C1**.

Interestingly, the fluorescence emission of **C1** was quite similar to that of **C2** in methyl alcohol (Figure 4). In other words, no ESIPT emission could be detected in methanol. Furthermore, as compared with the aprotic solvents, very weak ESIPT emission was observed for **C1** in ethyl alcohol. The results suggested that the occurrence of ESIPT was inhibited by the protic solvents for **C1**. This implied that intermolecular hydrogen bond effect between the solute and the protic solvent could limit the internal proton transfer at the excited state, which meant that the excited-state deprotonation instead of ESIPT occurred in the protic solvents.⁴⁵ It was interesting that the fluorescence intensity of ESIPT was lower than that of normal emission intensity. The intensity ratio of the emission bands, I_{N^*}/I_{E^*} (wherein I_{N^*} refers to the intensity of normal fluorescence emission, I_{E^*} is the representative of the intensity of ESIPT fluorescence emission) was roughly kept at 4–6 in various solvents. The fact that the normal fluorescence emission was prevailing implied that the existence of an appreciable energy barrier associated with ESIPT so that the decay $S_1 \rightarrow S_0$ of enol emission of **C1** became competi-

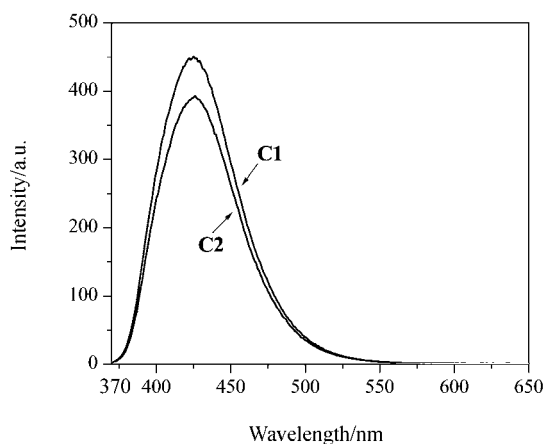


Figure 4 Fluorescence spectroscopy of **C1** and **C2** in methanol ($c=1 \times 10^{-5} \text{ mol}\cdot\text{L}^{-1}$). Ex: 350 nm, Slit window: Ex: 3 nm, Em: 3 nm.

tive.⁴⁶

The maximal emission wavelength and the fluorescence quantum yields of **C1** and **C2** are shown in Table 2. As compared with the absorption maxima, the normal fluorescence emission maxima of **C1** and **C2** exhibited obvious red-shift in polar solvents with respect to those in cyclohexane. Furthermore, the ESIPT fluorescence wavelength of **C1** exhibited larger red-shift in strong polar aprotic solvents than that in nonpolar aprotic solvents. This indicated that the excited singlet state was characterized with intramolecular charge transfer nature. **C1** and **C2** displayed low fluorescence quantum yields in various solvents. This was not surprising because it was generally accepted that the phenyl ring connecting with imino group was twisted in the Schiff base⁴⁵ and thus the molecular structure was not fully coplanar and conjugated, which could cause the reduction of the fluorescence quantum yields. It was worthy pointing out that an ultrafast spectroscopic experiment demonstrated that a very short lifetime (less than a picosecond) (n, π^*) existed in the single state of the enol form near the spectroscopic (π, π^*) state in salicylideneaniline, a typical Schiff base compound.⁴⁷ Thus, it was possible that **C1** and **C2** could have part of (n, π^*) nature in the single state and the fluorescence quantum yields could be further diminished as (n, π^*) transition was a forbidden transition. Table 2 showed that **C1** and **C2** had quite small fluorescence quantum yields in strong polar solvents, such as acetonitrile and acetone, which could be easily understood because the parent chromophore moiety of **C1** and **C2** (*i.e.* *N,N*-dimethylaminostilbene) was

a representative compound characterized with non-luminescent “twisted intramolecular charge transfer” phenomenon in strong polar solvents.⁴⁸

Theoretical calculation

Geometry parameters Both the electron transition and E-K phototautomerization led to the change of the molecular geometry parameters of the compound. The geometry optimization in S_0 and S_1 of E, K and TS (transition state) of **C1** and **C2** was performed and the parameters are listed in Tables 3 and 4 respectively. As our expectation, the transition state of **C2** could not be obtained, which in turn indicated the occurrence possibility of proton transfer for **C2** could be negligible in the excited state. While as sharp contrast, the existence of transition state for **C1** meant that it could be able to undergo ESIPT.

Seen from Table 3, the distances of H—O and H—N (in Schiff moiety) in transition state of **C1** (TS, namely six-member ring) was between those of E and K forms in both S_0 and S_1 states. While, the distance of O—N in transition state of **C1** was smaller than those of E and K forms in both S_0 and S_1 states. It was well accepted that the distance of O—N in transition state was the indication of hydrogen bond strength for the molecules which could undergo ESIPT. Hence, the shorter O—N revealed that the transition state was the structure with the strongest hydrogen bond strength. This was easily understood because in the transition state the H atom was shared by O and N atoms, so O atom and N atom had to be close to each other.⁴⁹

Table 2 The maximal fluorescence wavelength ($\lambda_{f,max}$) and fluorescence quantum yields (Φ) of **C1** and **C2** in various solvents

Solvent		C1	C2
Cyclohexane	$\lambda_{f,max}/nm$	388.0, 408.0, 533.0	385.0, 407.0
	Φ	0.0135	
Benzene	$\lambda_{f,max}/nm$	401.0, 424.0, 533.0	406.0, 424.0
	Φ	0.0454	0.0272
1,4-Dioxane	$\lambda_{f,max}/nm$	404.0, 425.0, 535.0	402.0, 424.0
	Φ	0.0160	0.0203
Tetrahydrofuran	$\lambda_{f,max}/nm$	402.0, 426.0, 534.0	401.0, 426.0
	Φ	0.0284	0.0300
Ethyl acetate	$\lambda_{f,max}/nm$	402.0, 425.0, 537.0	403.0, 425.0
	Φ	0.0277	0.0131
Methylene chloride	$\lambda_{f,max}/nm$	430.0, 555.0	430.0
	Φ	0.0103	0.0073
Acetonitrile	$\lambda_{f,max}/nm$	435.0, 546.0	434.0
	Φ	0.00254	0.00673
Acetone	$\lambda_{f,max}/nm$	428.0, 555.0	428.0
	Φ	0.00595	0.00833
Methanol	$\lambda_{f,max}/nm$	426.0	426.0
	Φ	0.0240	0.0106
Ethanol	$\lambda_{f,max}/nm$	429.0, 549.0	429.0
	Φ	0.0181	0.0108

Table 3 Most of relevant geometrical parameters (Å) of ground state at DFT and HF (in bracket) level and excited state in CIS level for **C1**

Structural parameter	Phototautomers in the ground state			Phototautomers in the excited state		
	E	TS	K	E*	TS*	K*
H—O	0.9987 (0.9547)	1.3029 (1.2718)	1.6292 (1.8676)	0.9567	1.2412	1.7957
H—N	1.7174 (1.8880)	1.1891 (1.1847)	1.0548 (1.0056)	1.8539	1.2108	1.0126
O—N	2.6204 (2.7119)	2.4228 (2.3850)	2.5557 (2.6568)	2.6907	2.3911	2.6385
C(1)—N—C(2)—C(3)	30.9997 (42.1840)	−15.7412 (33.2595)	1.1561 (29.7024)	−0.4762	−0.0128	−0.0590

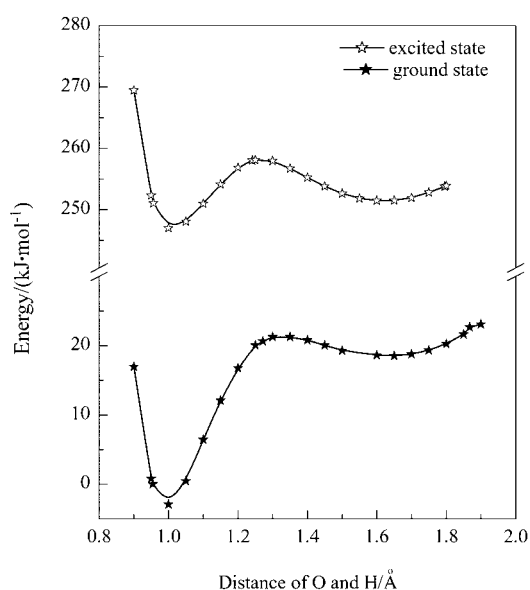
As shown in Table 4, in the S_0 and S_1 for the E form, the distance of H—N in Schiff moiety of **C2** was too long, even up to about 6.9 Å. It was well known that H-bond was short distance force in essence, hence the H-bond force between H and N should be inexistence in the E form for **C2**. On the other hand, due to no stretching effect of N for H, the distance of H—O in Schiff moiety of E form of **C2** was shorter than that of **C1** (*ca.* 0.0322 Å at DFT level). While as contrast, in the S_0 and S_1 for the K form, as compared with **C1**, the distance of H—N in Schiff moiety was shorter (*ca.* 0.1783 Å at DFT level), and the distance of H—O in Schiff moiety of K form was too much long as well (*ca.* 6.2 Å).

As we discussed, the E-K tautomerization brought a variation of the chemical bond length of phenol ring generally. For instance, the maximum of the difference between the bond lengths of phenolic ring in the enol form of **C1** was 0.0276 Å, while the value in the keto form of **C1** increased to 0.1202 Å, implying that aromaticity of this ring in the keto form was lost because of the internal proton transfer. **C2** showed such a larger change from E to K (0.0239 Å to 0.14479 Å) than **C1**, which suggested the difficulty on the ESIPT occurrence for **C2**. In addition, from E to E*, the electron excitation caused the reduction of aromaticity as well, and the distance of H—N bond of **C1** became shorter as 0.034 Å, so the internal proton transfer in the excited state was much easier than the ground state. Interestingly, as compared with HF method, the distances of O—N in the E and K forms of **C1** in the ground state were shorter by 0.0915 and 0.1011 Å respectively by DFT, which was found in **C2** as well. Whereas it is contrary in TS, the distances of O—N in the **C1** at HF level were shorter as 0.0378 Å.

Table 4 showed that the stable ground state geometry of E of **C1** had twisted bond N—C(2) by *ca.* 31° and 42° at B3LYP and HF level respectively. Dihedral angles $\angle C(1)NC(2)C(3)$ was decreased to *ca.* 1° and 30° respectively during E-K tautomerization, reflecting that the extent of molecular distortion was reduced, especially at DFT level. While in the excited state of **C1**, the tautomers remained essentially in the same plane. In a system with a great delocalization of π -electron, the torsion angle decided whether the molecule could be well-conjugated.⁵⁰ Consequently, the small twisted configuration in the excited state allowed the extension of the conjugated π -electron in all the molecular frame-

work, and the energy barrier in the ESIPT process caused by the bond twisting was reduced. It was favorable to undergo ESIPT for **C1**. While in contrast, although the molecular twist was reduced for **C2**, there still existed 10° twist of N—C(2). Furthermore, the dihedral angle of C(1)NC(2)C(3) did not exhibit great change in the ground state and the excited state. This in turn demonstrated that the occurrence of ESIPT for **C2** was quite difficult.

Energies The plots of the potential curves of internal proton transfer in S_0 and S_1 states of **C1** as a function of O—H distance were performed and presented in Figure 5, which showed clearly that an energy barrier existed for the internal proton transfer in S_0 and S_1 , and E form of **C1** was stable in the ground state. This implied that although the occurrence of GSIPT (E→K) should be very difficult, the reverse proton transfer process (K→E) could take place easily, which was much favorable for the ESIPT occurrence. Seen from Figure 5, we were surprised to observe that the energy of K* form in the excited state was a little higher than that of E*. As reported, ESIPT took place in **C3** through a barrierless process,³² and the energy of K* was lower than that of E*. Our results further confirmed that an acceptable energy barrier existence increased the

**Figure 5** The internal proton-transfer reaction potential energy curves relaxed along the O—H distance for ground and excited state.

difficulty on the ESIPT occurrence for **C1**. With the RRKM (Rice-Ramsperger-Kassel-Marcus) theory, the internal proton transfer rate constant (k) of **C1** in the excited state was calculated as $9.831 \times 10^{11} \text{ s}^{-1}$, which was remarkably lower than that of **C3** ($2.045 \times 10^{15} \text{ s}^{-1}$, the data was calculated in our lab as well). This confirmed that as compared with **C3**, the chromophore group did make the ESIPT occur difficultly for **C1**.

Table 5 presented the relative energy parameters of S_0 and S_1 states of **C1** at different calculation levels. ΔE (energy difference between E and K) showed clearly that keto form has a higher energy than E form in S_0 state as the aromatic ring was broken by proton transfer. The ΔE_d^\ddagger (direct reaction energy barrier) demonstrated that an energy barrier existed between the two tautomers of **C1**, which indicated that the proton transfer was an endothermic process in both S_0 and S_1 states of **C1**. Interestingly, the ΔE_d^\ddagger (reverse reaction energy barrier) in the ground state was much larger than that in the excited state, which meant that the ESIPT occurrence was easier than the ground state intramolecular proton transfer (GSIPT). While, ΔE_r^\ddagger (4.3185 and -2.0435 kJ/mol at DFT//DTT and DFT//HF calculative levels) in ground state implied that the occurrence of the reverse proton transfer process (namely from K \rightarrow E) easily took place, which was absolutely favorable for ESIPT for **C1**. As shown in Table 6, **C2** had nearly two times of the

energy difference between E and K in ground state (ΔE) (ca. 37.6727 kJ/mol) as that of **C1** (ca. 19.4475 kJ/mol). Furthermore, the difference in excited state reached approximately three times (6.9841 and 23.7338 kJ/mol) of that of **C1**. This showed that the occurrence of proton transfer in the ground and excited states became much harder for **C2**, particularly in the excited state. This is why we could not detect ESIPT fluorescence emission of **C2** in the experimental survey.

Frontier orbitals, atomic charge and dipole moment The electron distribution of the frontier orbitals reflects the electron transition characteristics. Seen from Figure 6, the HOMO and LUMO of **C1** and **C2** exhibited π -type symmetry. From HOMO to LUMO, the electron density distribution displayed the transfer from *N,N*-dimethylamino stilbene chromophore to Schiff base moiety. Thus, the phenolic ring had larger electron density in the S_1 excited state, which was the driving force for the occurrence of proton transfer for **C1** in the excited state. Hence, the HOMO \rightarrow LUMO transition could be ascribed to $\pi\rightarrow\pi^*$ excitation with internal charge transfer character.^{51,52}

The Mulliken net atomic charge population of the key atoms of **C1** is presented in Figure 7. Remarkably, as our expectation, hydrogen atom had high positive charge, which indicated that it was a "real proton" transfer if ESIPT or GSIPT took place. Interestingly, the

Table 4 Most of relevant geometrical parameters (Å) of ground state at DFT and HF (in bracket) level and excited state in CIS level for **C2**

Structural parameter	Phototautomers in the ground state		Phototautomers in the excited state	
	E	K	E*	K*
H—O	0.9665 (0.9429)	6.2664 (6.2452)	0.9429	6.0161
H—N	6.9631 (6.9266)	1.0108 (0.9928)	6.9206	0.9949
O—N	6.4183 (6.3743)	6.4430 (6.3832)	6.3656	6.3869
$\angle C(1)NC(2)C(3)$	$-146.6797 (-139.9969)$	$-146.4282 (-151.0897)$	170.2535	173.0105

Table 5 The calculated ground and excited state relative potential energy (kJ/mol) and energy barrier of different phototautomers with different method^a

State	Method	E_E	E_{TS}	E_K	ΔE	ΔE_d^\ddagger	ΔE_r^\ddagger
Ground	DFT//DFT	0	23.756	19.439	19.439	23.756	4.317
	DFT//HF	23.364	44.006	46.049	22.685	20.642	-2.043
Excited	TDDFT//CIS	274.425	281.406	277.148	2.723	6.981	0.0744

^a The energies of E at DFT//DFT as the reference point.

Table 6 The calculated ground and excited state relative potential energy (kJ/mol) and energy barrier of different tautomers with different method^a

State	Method	E_E	E_{TS}	E_K	ΔE	ΔE_d^\ddagger	ΔE_r^\ddagger
Ground	DFT//DFT	0	—	34.596	34.596	—	—
	DFT//HF	19.769	—	57.425	37.656	—	—
Excited	TDDFT//CIS	278.740	—	302.463	23.723	—	—

^a The energies of E at DFT//DFT as the reference point.

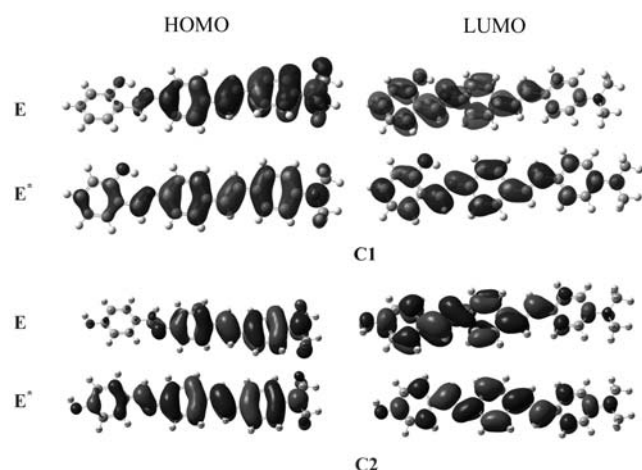


Figure 6 The frontier orbital of enol form in the ground state and the excited state for **C1** and **C2**.

positive charge of hydrogen experienced increasing and then decreasing during intramolecular proton transfer both in ground and excited states, reaching the maximum at transition state because of largest hydrogen-bonding strength. While as E was excited to E*, part of negative charge was transferred from the hydroxyl to the imino group, which resulted in the change of the “force balance” of hydrogen bond. Consequently the negative charge of proton donor (O) decreased (less basicity, more acidity), and the negative charge of proton receptor (N) increased (less acidity, more basicity), which enhanced the change of geometry in the excited state⁵³ and promoted the ESIPT occurrence for **C1**. Table 7 showed that the dipole moments centralized on the X-dimension and the electronic transition led to the changes in the charge distribution, which was accompanied by the increasing of the molecular dipole moments in the excited state.

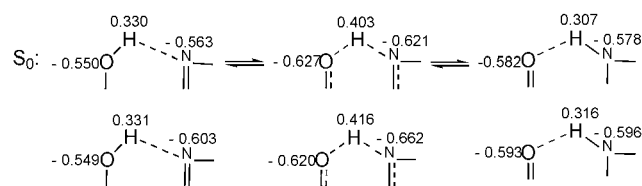


Figure 7 The calculated Mulliken net atomic charge population of the key atoms of **C1**.

As shown in Table 8, for **C2**, as E was excited to E*, negative charge of oxygen in hydroxyl was reduced and the negative charge of nitrogen in imino group was enhanced. On the other hand, tiny charge change was not enough for ESIPT occurrence between hydroxyl and imino groups. As compared with **C1**, owing to the great changes of dipole moments on the X-dimension in both the ground state and the excited state, the dipole moment of **C2** of E form was lowered, but the dipole moment of K form was enhanced greatly, thus the dipole moment difference of tautomers of **C2** exhibited much

Table 7 Dipole moment of phototautomers of **C1** in the ground and excited states

State	Phototautomer	X	Y	Z	Total
Ground	E	-3.8943	-1.9777	-0.6309	4.4130
	TS	5.5664	-2.5398	0.5185	6.1404
	K	-6.2508	2.5965	1.5526	6.9444
Excited	E*	5.8273	-2.0193	0.1674	6.1695
	TS*	-6.1012	-2.4922	0.2330	6.5947
	K*	6.5826	-2.8544	0.2763	7.1801

Table 8 Calculated Mulliken net atomic charges (*e*) of the key atoms for **C2**

State	E			K		
	O	H	N	O	H	N
Ground	-0.551	0.320	-0.491	-0.529	0.276	-0.613
Excited	-0.543	0.315	-0.518	-0.513	0.273	-0.610

larger changes in both the ground and excited state than **C1** (2.5314, 1.0106 for **C1**; *ca.* 8.3089, 8.9623 for **C2**, see Tables 7 and 9). This meant that so large change of charge geometry occurred if the internal proton transfer took place, which in turn indicated the possibility for **C2** to undergo GSIPT or ESIPT could be very negligible.

Table 9 Dipole moment of phototautomers of **C2** in the ground and excited states

State	Phototautomer	X	Y	Z	Total
Ground	E	1.0806	2.4880	-0.8919	2.8554
	K	-11.1636	-0.0370	-0.1153	11.1643
Excited	E*	-2.6772	2.3623	-0.1099	3.5721
	K*	-12.5314	0.2719	0.0403	12.5344

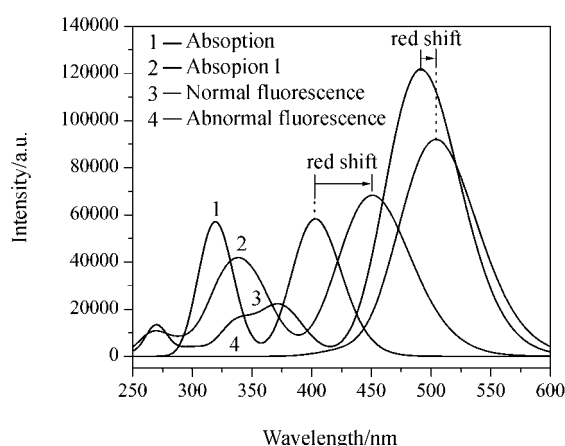
Spectra

The calculated absorption spectra, normal fluorescence spectra and “abnormal” fluorescence spectra of tautomer species of **C1** are present in Figure 8, which were obtained with the Lorentz broadening of the anterior twenty excitation energies (ΔE) and corresponding oscillator strengths (*f*). The peak wavelengths of the spectra are listed in Table 10, which equaled to the corresponding singlet-singlet transition energies (ΔE). Herein, the values of absorption referred to the vertical transition from S_0 states to the Franck-Condon S_1 states, while the values from S_1 states to the corresponding Franck-Condon S_0 could be assigned to the fluorescence emission,⁵⁴ which were red-shifted with respect to the absorption. As shown in Table 10, most of them could be contributed by the electron excitation from HOMO to LUMO, in which the weightages were more than 78% with the largest oscillator strengths in normal fluorescence (*f*, 1.6821).

Interestingly, the absorption maxima were consistent with those in solvents. This further demonstrated that

Table 10 Calculated absorption and fluorescence wavelengths (in nm), singlet-singlet transition energies (in eV) and the weightage of the most important microstate (H: HOMO, L: LUMO) in the first excited state for **C1** at the TDDFT//HF and TDDFT//CIS level

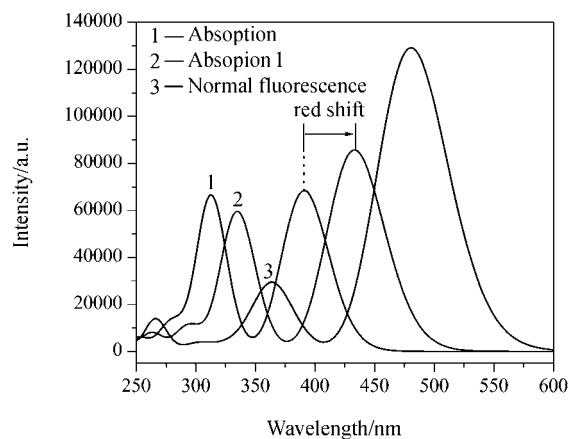
Spectra		$\Delta E/eV$	λ/nm	f	Transition
Absorption	1	3.08	403.1	0.8057	H→L: 92%
	2	3.83	323.4	0.5788	H-1→L: 72%; H→L+1: 17%
	3	4.00	310.2	0.3087	H→L+1: 69%; H-1→L: 13%
Normal fluorescence	1	2.52	491.4	1.6821	H→L: 78%
	2	3.31	374.4	0.2903	H-1→L: 68%; H→L+1: 24%
	3	3.67	337.9	0.2016	H-2→L: 43%; H→L+1: 36%
Abnormal fluorescence	1	2.46	504.1	1.2698	H→L: 82%
	2	2.90	427.7	0.0357	H-1→L: 81%; H→L+1: 6%
	3	3.05	406.2	0.0000	H-3→L: 93%

**Figure 8** Calculated absorption (absorption: TDDFT//HF; absorption 1: TDDFT//DFT) and fluorescence spectra (TDDFT//CIS) for **C1**.

the absorption spectroscopy was almost independent of the polarity of media. However, the calculated maximal ESIPT fluorescence maximum was blue-shifted with respect to the experimental value (*ca.* 30 nm). This in turn implied that ESIPT fluorescence emission was sensitive to the polarity of media. As shown in Table 6, the calculated large Stokes shift of ESIPT fluorescence emission (101.0 nm) was observed, which meant the large change of geometry in the excited state such as the strong deformations of bond distances. It was worthy mentioning that Stokes shifts of ESIPT reached 140–160 nm in various solvents in experiments. It was strong evidence that the larger change of geometry in the excited state happened in solvents, and it confirmed that the ESIPT fluorescence was more sensitive to solvent polarity for **C1**.

Figure 9 showed the calculated absorption and fluorescence spectroscopy of **C2**. No ESIPT fluorescence spectroscopy was obtained. Table 11 listed the calculated data of the absorption and normal fluorescence spectroscopy of **C2**. H→L transition had the largest f value (0.9463, 1.7832 for the absorption spectroscopy and the fluorescence spectroscopy respectively) and the

biggest weightage (90%, 78% for the absorption spectroscopy and the fluorescence spectroscopy respectively). Obviously, it was further demonstrated that the absorption was characterized with $\pi \rightarrow \pi^*$ electron excitation. Interestingly, there was nice agreement between the calculated and experimental values of the maximal absorption wavelength of **C2** as well, which implied the weak dependence of the absorption maxima on the polarity of media. Furthermore, the calculated maximal absorption maximum of **C2** exhibited approximate 10 nm blue-shift with respect to that of **C1**, which was observed in the experimental survey as well.

**Figure 9** Calculated absorption (absorption: TDDFT//HF; absorption 1: TDDFT//DFT) and fluorescence spectra (TDDFT//CIS) for **C2**.

We further calculated the absorption spectra of **C1** and **C2** at DFT optimized level respectively. Figures 7 and 8 (denoted as absorption 1) showed that DFT yielded higher transition energy due to the geometrical difference (seen in Table 1). The absorption spectra at DFT level were red-shifted by about 50 nm for **C1** and **C2** with respect to HF method.

We shall point out that the calculated maximal normal fluorescence emission wavelength of **C1** and **C2** was not in well agreement with the experimental values. In principle, basing on the molecular equilibrium ge-

Table 11 Calculated absorption and fluorescence wavelengths, singlet-singlet transition energies and the weightage of the most important microstate (H: HOMO, L: LUMO) in the first excited state for **C2** at the TDDFT//HF and TDDFT//CIS level

Spectra		$\Delta E/eV$	λ/nm	f	Transition
Absorption	1	3.17	390.9	0.9463	H→L: 90%
	2	3.95	313.6	0.7733	H-1→L: 54% ; H→L+1: 37%
	3	4.02	308.8	0.1527	H→L+1: 45% ; H-1→L: 23%
Normal Fluorescence	1	2.58	480.5	1.7832	H→L: 78%
	2	3.40	364.5	0.3932	H-1→L: 56% ; H→L+1: 39%
	3	3.71	334.5	0.0545	H-3→L: 40% ; H-2→L: 23%

ometries in S_1 state, the emission energy can be predicted using the TDDFT at B3LYP level as the method which could well calculate the absorption energy. Although the calculation using TDDFT at B3LYP level was well agreement with the experimental results on absorption energy, which was confirmed in the present study again, the theoretic emission energy with this method generally was not satisfactory. This could be understood from the following reasons. The fluorescence emission occurred on the molecular electronic excited states whose geometrical and electronic structures were more complicated than those on the ground state, and the physical mechanism of fluorescence emission was more intricate as well, resulting in the enhancement of the difficulty of theoretical simulation. Furthermore, although TDDFT method has higher calculation precision than TDHF (time-dependent Hartree-Fock) and CIS method because of the introduction of the exchange-correlation (XC) functional, it had many limitations. One of the most important factors was that the exact expression of XC functional was unknown, thus the approximate expression of them had to be adjusted or fitted with experimental values, and hence TDDFT method could bring out a great deviation if it was used to calculate the excited state molecule. Wu *et al.* pointed out that the most important factor of the emission energy calculation was the proportion of HF exchange correlation part (x) in the XC functional.⁵⁵ B3LYP with 20% HF exchange energy in its exchange term would produce a great deviation because of the less consideration of non-dynamic correlation energy, even as high as 0.5 eV above.

Conclusions

In this article, we have presented the synthesis and characterization of new dyes linked with imino group. Comprehensive investigation on the spectroscopic properties was performed in theory and experiment. The results demonstrated that the substituted position of the phenol hydroxyl group had shown a close interrelationship with their spectral properties, particularly in ESIPT. As compared with **C2** carrying substituted phenol hydroxyl group in 4-position, **C1** bearing substituted phenol hydroxyl group in 2-position exhibited not only longer absorption maxima, but obvious ESIPT fluores-

cence emission in aprotic solvents. While, non-ESIPT fluorescence emission for **C2** could be ascribed to the difficulty on the formation of an acceptable transit state due to long distance of C=N (imino group) and phenol hydroxyl group. As contrast, a reasonable six-member ring could lead to an appreciable energy barrier for **C1**. The existences of a transit state and an acceptable energy barrier during ESIPT process for **C1** were demonstrated with theoretical calculation. Furthermore, the calculated results showed the presence of too high energy barrier during proton transfer in both the ground state and the excited state to proceed ESIPT for **C2**. The comparison of the structural parameters, the frontier molecular orbitals analysis, and the atomic charge and dipole moments of phototautomers of **C1** and **C2** suggested clearly that the possibility of ESIPT occurrence for **C1** was much higher than that for **C2**, which was confirmed in the experiment. ESIPT was difficult to accomplish for **C2**. While as compared with **C3**, the existence of energy barrier demonstrated in turn that chromophore part increased somewhat difficulty on the occurrence of ESIPT for **C1** and its proton rate was lowered in the excited state.

Acknowledgement

We thank supports to the Key Laboratory of Functional Crystals and Laser Technology, Technical Institute of Physics and Chemistry, Chinese Academy of Sciences.

References

- Sardar, P.; Samata, S.; Maity, S. S.; Dasgupta, S.; Ghosh, S. *J. Phys. Chem. B* **2008**, *112*, 3451.
- Wu, Y.; Peng, X.; Fan, J.; Gao, S.; Tian, M.; Zhao, J.; Sun, S. *J. Org. Chem.* **2007**, *72*, 62.
- Barbatti, M.; Aquino, A. J. A.; Lischka, H.; Schriever, C.; Lochbrunner, S.; Riedle, E. *Phys. Chem. Chem. Phys.* **2009**, *11*, 1406.
- Chen, K.; Cheng, Y.; Lai, C.; Hsu, C.; Ho, M.; Lee, G.; Chou, P. *J. Am. Chem. Soc.* **2007**, *129*, 4534.
- Doroshenko, A. O.; Posokhov, E. A.; Verezubova, A. A.; Pyagina, L. M.; Skripkina, V. T.; Shershukov, V. M. *Photochem. Photobiol. Sci.* **2002**, *1*, 92.
- Lukeman, M.; Veale, D.; Wan, P.; Munasinghe, V. R. N.; Corrie, J. E. T. *Can. J. Chem.* **2004**, *82*, 240.

- 7 Coe, J. D.; Levine, B. G.; Martinez, T. J. *J. Phys. Chem. A* **2007**, *111*, 11302.
- 8 Peng, X.; Wu, Y.; Fan, J.; Tian, M.; Han, K. *J. Org. Chem.* **2005**, *70*, 10524.
- 9 Solntsev, K. M.; Sullivan, E. N.; Tolbert, L. M.; Ashkenazi, S.; Leiderman, P.; Huppert, D. *J. Am. Chem. Soc.* **2004**, *126*, 12701.
- 10 Toele, P.; Zhang, H.; Glasbeek, M. *J. Phys. Chem. A* **2002**, *106*, 3651.
- 11 Roberts, E.; Dey, J.; Warner, I. M. *J. Phys. Chem. A* **1997**, *101*, 5296.
- 12 Fores, M.; Duran, M.; Sola, M.; Adamowicz, L. *J. Comput. Chem.* **2009**, *21*, 257.
- 13 Helmut, G.; Sumit, K.; Thomas, W.; Phalguni, C. *J. Phys. Chem. A* **2006**, *110*, 2587.
- 14 Lim, S.; Seo, J.; Park, S. *J. Am. Chem. Soc.* **2006**, *128*, 14542.
- 15 Shen, F.; Xia, H.; Zhang, C.; Lin, D.; He, L.; Ma, Y. *J. Phys. Chem. B* **2004**, *108*, 1014.
- 16 Sun, W.; Li, S.; Hu, R.; Qian, Y.; Wang, S.; Yang, G. *J. Phys. Chem. A* **2009**, *113*, 5888.
- 17 Rodembusch, F.; Campo, L.; Stefani, V.; Rigacci, A. *J. Mater. Chem.* **2005**, *15*, 1537.
- 18 Park, S.; Kim, S.; Seo, J.; Park, S. *Macromol. Res.* **2008**, *16*, 385.
- 19 Chou, P.; Chen, Y.; Yu, W.; Cheng, Y. *Chem. Phys. Lett.* **2001**, *340*, 89.
- 20 Kim, S.; Chang, D.; Park, S. *Macromolecules* **2002**, *35*, 6064.
- 21 Rodembusch, F.; Leusin, F.; Medina, L.; Brandello, A.; Stefani, V. *Photochem. Photobiol. Sci.* **2002**, *1*, 92.
- 22 Taneda, M.; Kodama, Y.; Eda, Y.; Koyama, H.; Kawato, T. *Chem. Lett.* **2007**, *36*, 1410.
- 23 Abella, C. A. M.; Rodembusch, F.; Stefani, V. *Tetrahedron Lett.* **2004**, *45*, 5601.
- 24 Holler, M.; Campo, L.; Brandelli, A.; Stefani, V. *J. Photochem. Photobiol. A: Chem.* **2002**, *149*, 217.
- 25 Yu, W.; Cheng, C.; Cheng, Y.; Wu, P.; Song, Y.; Chi, Y.; Chou, P. *J. Am. Chem. Soc.* **2003**, *125*, 10800.
- 26 Qian, Y.; Li, S.; Zhang, G.; Wang, S.; Xu, H.; Li, C.; Li, Y.; Yang, G. *J. Phys. Chem. B* **2007**, *111*, 5861.
- 27 Chang, D.; Kim, S.; Park, S. *Macromolecules* **2000**, *33*, 7223.
- 28 Kim, S.; Park, S.; Yoshida, I.; Kawai, H.; Nagamura, T. *J. Phys. Chem. B* **2002**, *106*, 9291.
- 29 Sahoo, S.; Rati, K.; Baral, M.; Kanungo, B. *J. Photochem. Photobiol. A* **2007**, *188*, 298.
- 30 Zio, M.; Kubicki, J.; Maciejewski, A.; Naskr, R.; Grabowska, A. *Chem. Phys. Lett.* **2003**, *369*, 80.
- 31 Fita, P.; Luzina, E.; Dziembowska, T.; Kopec, D.; Piatkowski, P.; Radzewicz, C.; Grabowska, A. *Chem. Phys. Lett.* **2005**, *416*, 305.
- 32 Zgierski, M. Z.; Grabowska, A. *J. Chem. Phys.* **2000**, *113*, 7845.
- 33 Perrin, D. D.; Armarego, W. L. F.; Perrin, D. R. *Purification of Laboratory Chemicals*, Pergamon Press, New York, **1966**.
- 34 Eaton, D. F. *Pure Appl. Chem.* **1988**, *60*, 1107.
- 35 Fischer, M.; Georges, J. *Chem. Phys. Lett.* **1996**, *260*, 115.
- 36 Maus, M.; Retigg, W.; Bonafoux, D.; Lapouyade, R. *J. Phys. Chem. A* **1999**, *103*, 3388.
- 37 Zgierski, M. Z.; Grabowska, A. *J. Chem. Phys.* **2000**, *112*, 14.
- 38 Yi, P.; Liang, Y.-H.; Cao, C. *Chem. Phys.* **2005**, *315*, 297.
- 39 Liang, Y.-H.; Yi, P.-G. *Chem. Phys. Lett.* **2007**, *438*, 173.
- 40 Chen, D.-Z.; Wang, D.-P.; Zhang, H.; Tang, B. *Chem. Phys. Lett.* **2002**, *353*, 119.
- 41 Han, D.; Gao, P. *The Basis of Chemical Kinetics*, Peking University Press, Beijing, **1998** (in Chinese).
- 42 Cavallini, G.; Massarani, E. *US 2878291*, **1958**.
- 43 Falkovskaia, E.; Pivovarenko, V. G.; Del Valle, J. C. *J. Phys. Chem. A* **2003**, *107*, 3316.
- 44 Chiang, W.-Y.; Laane, J. *J. Phys. Chem.* **1995**, *99*, 11823.
- 45 Chou, P.-T.; Huang, C.; Pu, S.; Cheng, Y.; Liu, Y.; Wang, Y.; Chen, C. *J. Phys. Chem. A* **2004**, *108*, 6452.
- 46 Yu, W.; Cheng, C.; Cheng, Y.; Wu, P.; Song, Y.; Chi, Y.; Chou, P. *J. Am. Chem. Soc.* **2003**, *123*, 10800.
- 47 Okabe, C.; Nakabayashi, T.; Inokuchi, Y.; Nishi, N.; Sekiya, H. *J. Chem. Phys.* **2004**, *121*, 9436.
- 48 Letard, J. F.; Lapouyade, R.; Rettig, W. *Chem. Phys.* **1994**, *186*, 119.
- 49 Fores, M.; Duran, M.; Sola, M. *Chem. Phys.* **1998**, *234*, 1.
- 50 Yesylevskyy, S. O.; Klymchenko, A. S. *J. Mol. Struct.: Thermochem.* **2005**, *755*, 229.
- 51 Chen, X.; Chen, J.; Li, Q. *Chin. J. Org. Chem.* **2008**, *28*, 6 (in Chinese).
- 52 Kakkar, R.; Katoch, V. *J. Mol. Struct.: Theochem.* **2002**, *578*, 169.
- 53 Moller, S.; Andersen, K. B. *Chem. Phys. Lett.* **1998**, *219*, 51.
- 54 Wang, Y.; Wu, G. *Acta Phys.-Chim. Sim.* **2008**, *24*, 4 (in Chinese).
- 55 Wang, Y.; Wu, G. *Acta Phys.-Chim. Sim.* **2007**, *23*, 1831 (in Chinese).

(E0911181 Zhao, C.; Dong, H.)